Applied Physics B (2022) 128:35
https://doi.org/10.1007/s00340-022-07765-3

Applied Physics B
Lasers and Optics

Tunable squared patch-based graphene metasurface infrared polarizer

Vishal Sorathiya[1] · Sunil Lavadiya[1] · Bijraj Singh Parmar[2] · Saumya Baxi[2] · Taher Dhankot[2] · Osama S. Faragallah[3] · Mahmoud M. A. Eid[4] · Ahmed Nabih Zaki Rashed[5]

Received: 13 March 2021 / Accepted: 20 December 2021 / Published online: 30 January 2022

Abstract

In this manuscript, patch-shaped graphene metasurface polarizer has been numerically investigated for the far-infrared frequency spectrum. We have identified the resonance response of the proposed polarizer by changing the physical dimensions of the proposed polarizer. The proposed polarizer structure has been investigated for the 1–20 THz of the frequency range. The different physical parameters such as phase variation, polarization conversion rate, reflectance, and transmittance have been investigated for the proposed polarizer structure. Graphene-based polarizer structures are formed with the squared patched geometry, and its complementary condition has been investigated to identify the polarization effect's behavior. The proposed polarizer device is tunable by various values of graphene chemical potential. The calculated polarization conversion rate (PCR) is >0.9 for the resonating point, showing the linear to circular polarization conversion. The proposed structure works as a tunable polarizer device where the graphene sheet properties can be controlled from external sources. A resonating band of the polarization effect has been identified from the numerical results of polarization conversion rate and cross-polarization behavior. The phase variation is observed between $-180°$ and $180°$ in the graphene patch-based polarizer structure. In contrast, the polarizer structure's complementary geometry generates the phase variation between $100°$ and $180°$. The proposed polarizer can be easily fabricated using conventional methods as it does not require a complex structure to engrave the graphene sheet. Ultrathin design and tunable properties of the polarizer structure can be used in many photonics and optoelectronics applications.

✉ Ahmed Nabih Zaki Rashed
ahmed_733@yahoo.com

Vishal Sorathiya
vishal.sorathiya9@gmail.com

Sunil Lavadiya
splavadiya@gmail.com

Bijraj Singh Parmar
bj08222@gmail.com

Saumya Baxi
sombaxi@gmail.com

Taher Dhankot
taherdhankot52@gmail.com

Osama S. Faragallah
o.salah@tu.edu.sa

Mahmoud M. A. Eid
m.elfateh@tu.edu.sa

[1] Department of Information and Communication Technology, Marwadi University, Rajkot, Gujarat 360003, India

[2] Department of Electronics and Communication Engineering, Marwadi Education Foundation's Group of Institutions, Rajkot, Gujarat 360003, India

[3] Department of Information Technology, College of Computers and Information Technology, Taif University, P.O. Box 11099, Taif 21944, Saudi Arabia

[4] Department of Electrical Engineering, College of Engineering, Taif University, P.O. Box 11099, Taif 21944, Saudi Arabia

[5] Electronics and Electrical Communications Engineering Department, Faculty of Electronic Engineering, Menoufia University, Menouf 32951, Egypt

1 Introduction

Graphene material was developed at the University of Manchester by Andre Geim and co-workers by employing the Scotch Tape method [1]. Graphene, the two-dimensional structure, has shown an astronomical rise in the field of physics. It has found usage in a broad range of applications [2]. This 'miracle material' has properties that are second to none. Some of its unique and supreme properties are higher electrical and thermal conductivity, ease of being functionalized chemically. In addition, graphene shows unmatched elasticity and transparency [3]. It has also shown unique properties such as quantum hall effect (QHE) and high carrier mobility [4]. Different techniques such as atomic force microscopy, X-ray diffraction, scanning tunneling microscopy and Raman spectroscopy are employed to study and research different types of graphene [5]. In addition, graphene is an eco-friendly material, so they have found uses for biological purposes [6]. The realization of graphene's derivatives has opened new horizons for its widespread usage in various industries [4]. Exhibiting properties that are unlikely to be found in nature, metamaterials have attracted a lot of traction in the field of electromagnetics and photonics. Metamaterials have shown different responses to light, acoustic waves, etc. [7].

Metasurfaces that have reduced dimensions compared to metamaterials have gained a lot of attraction because of their feasibility for realization and showcase excellent light modeling abilities compared to those being offered by the typical planar interfaces [8]. They are two-dimensional (2-D) structures and are defined as thin and dense arrays of structural elements. They possess unique properties under their resonant behavior [9]. Metasurfaces are easily fabricated and are light in weight. They have the unique property of manipulating electromagnetic waves in optical and microwave frequencies [10]. Important applications of this material made by resonant meta-atoms are lenses, holograms, and so on. In addition, the frequency selective surfaces (FSSs) used in radiophysics are the older version of the current age optical metasurfaces [11–14]. Polarizer plays a pivotal role in optical systems and networks. Far-infrared polarizers will play an essential role in various applications [15, 16]. Talking about far-infrared polarizers, there is a shortage of useful and low-cost polarizers in this frequency [17].

In this research, we have proposed the numerical results of the graphene-based polarizer with tunable behavior over a range of 1–20 THz far-infrared spectrum. We have identified the polarizer effects in terms of transmittance, reflectance, phase variation, and polarization conversion rate (PCR). We have tried to provide the basic approach to design a graphene-based polarizer. We have identified the appropriate resonance points where the wave is transmitted maximum and polarization generates. Second, we have identified the relationship between resonance frequency and the size of the polarizer structure. We have identified the three equations that will help decide the structure's size for the specific resonance frequency. Third, we have set the polarizer structure's dimension constant and presented the results of the various physical parameters. In the third section, the polarizer structure's tunable behavior, the effect of graphene patch size, polarization conversion rate, and phase variation are presented and discussed.

2 Graphene-based polarizer

A schematic of the graphene-based metasurface polarizer has been presented in Fig. 1. The periodic view of the normal structure has been shown in Fig. 1a. In the proposed structure graphene patch has been placed at the center of the overall design. The silica material has been placed on the bottom of the single-layered graphene patch. The second polarizer geometry has been designed by considering the complementary geometry of the graphene over periodic axis X and Y, as represented in Fig. 1b. In the proposed polarizer structure the dimensions are defined as $H = 0.2$ µm, $L = 25$ µm, $g_1 = g_2 = 12.5$ µm. The design shown in Fig. 1a was named here as a normal graphene-based polarizer (NGP), and the design shown in Fig. 1b was named a complimentary graphene-based polarizer (CGP). NGP and CGP were numerically investigated by considering periodic boundary conditions over the X- and Y-axis, while the wave was imparting from the Z direction. We have used the finite-element method (FEM)-based computational techniques for simulating the structure.

2.1 Graphene as surface conductivity model

The conductivity model of the graphene has been taken as per the equation suggested using the Kubo formula [18]. The conductivity model of the graphene sheet can be presented by intramodal and intermodal conductivity equation as shown in Eqs. (2–4). The graphene material permittivity is presented in Eq. (1):

$$\varepsilon(\omega) = 1 + \frac{\sigma_s}{\varepsilon_0 \omega \Delta}, \tag{1}$$

$$\sigma_{\text{intra}} = \frac{-je^2 k_B T}{\pi \hbar^2 (\omega - j2\Gamma)} \left(\frac{\mu_c}{k_B T} + 2\ln\left(e^{-\frac{\mu_c}{k_B T}} + 1 \right) \right), \tag{2}$$

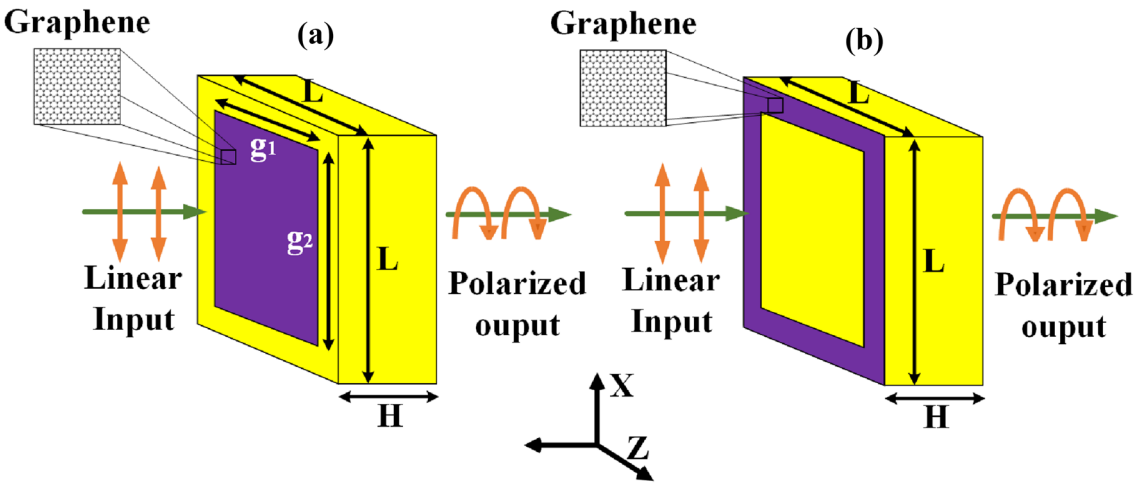

Fig. 1 Schematic of the polarizer structure. Three-dimensional view of **a** NGP and **b** CGP. Dimensions of the structure are set as $H=5$ µm, $L=25$ µm, $g_1=g_2=12.5$ µm. The graphene thickness is set as 0.3 nm (consider the graphene thickness in surface conductivity value equation)

$$\sigma_{\text{inter}} = \frac{-je^2}{4\pi\hbar}\ln\left(\frac{2|\mu_c| - (\omega - j2\Gamma)\hbar}{2|\mu_c| + (\omega - j2\Gamma)\hbar}\right), \tag{3}$$

$$\sigma_s = \sigma_{\text{inter}} + \sigma_{\text{intra}}. \tag{4}$$

We can control the graphene chemical potential using external gate bias voltage. The relation between external biased voltage (V_b) and Fermi chemical potential (μ_c) is defined as $\mu_c = \hbar v_F\sqrt{\pi C V_b}$. Here, the capacitance is defined as $C = \varepsilon_0\varepsilon_d/H$, where ε_0 is the free space permittivity, ε_d is the silica material permittivity with a value of 2.25. H (0.2 µm) represents silica material thickness. Complex value results can be derived from the graphene conductivity equation. The solution of the graphene conductivity equation affecting as reactive and resistive behavior of the structure. Under the calculation of the graphene sheet in FEM simulation, the graphene thickness is set as 0.3 nm. The values of the surface current destiny are defined as $J_y = E_y\sigma_s$ and $J_x = E_x\sigma_s$ under the periodic boundary conditions.

3 Calculation of resonance effect

The graphene-based photonic structures can be tunable using different external parameters. The effect of the graphene chemical potential/fermi voltage on conductivity values of the graphene is shown in Fig. 2. It is observed that the real and imaginary parts of the graphene conductivity vary for the large band of THz spectrum. It is also required to identify the proper dimension of the polarizer structure for a specific frequency range. The transmittance coefficient is defined as $T_{ij} = \left|E_j^{\text{Reflec}}/E_i^{\text{Inc}}\right|(i,j=x,y)$, where $E_j^{\text{Reflec}}(j=x,y)$ is the x or y component of the reflected wave and $E_j^{\text{Inc}}(j=x,y)$ is the x or y component of the incident wave [19]. The phase is defined as $\Phi_{ij} = \arg\left(E_j^{\text{Reflec}}/E_i^{\text{Inc}}\right)(i,j=x,y)$. The phase difference between the input incident and the output reflected wave is presented as $\Delta\Phi = \Phi_{xx} - \Phi_{yy}$. While in the case of cross-polarization, phase difference is presented by $\Delta\Phi = \Phi_{xx} - \Phi_{xy}$. We have calculated the behavior of the proposed single-layer graphene-based NGP and CGP structure over a 1–20 THz range of frequency. Resonance effects over 1–20 THz have been identified for the different values of structure size L.

The amplitude variation of T_{xx} and R_{xx} have been presented in Fig. 3a and b for the NGP structure. Similarly, amplitude variation of T_{xx} and R_{xx} has been illustrated in Fig. 3c and d for CGP structure. The specific resonance points have been generated over 1–20 THz of the frequency spectrum for NGP and CGP structures, as shown in Fig. 3. In the graphene-based structure, resonating points are generated due to dipole moments created at the edges of the graphene sheet. We have calculated the approximate function which can use to identify the resonance frequency and structure size. We have identified the three relationship functions between L and f. The initial resonating frequency of the graphene depends on the length and width of the structure by considering the function $f_r \cong \sqrt{E_f/L}$ [20], where, $E_f = \mu_c =$ Fermi energy of the graphene sheet. From this equation by identifying the resonance peak at specific fermi voltage, we have identified the initial dimensions of the structure as $H=5$ µm, $L=25$ µm, and $g_1=g_2=12.5$ µm. Later on, we have simulated the structure for the different conditions of the

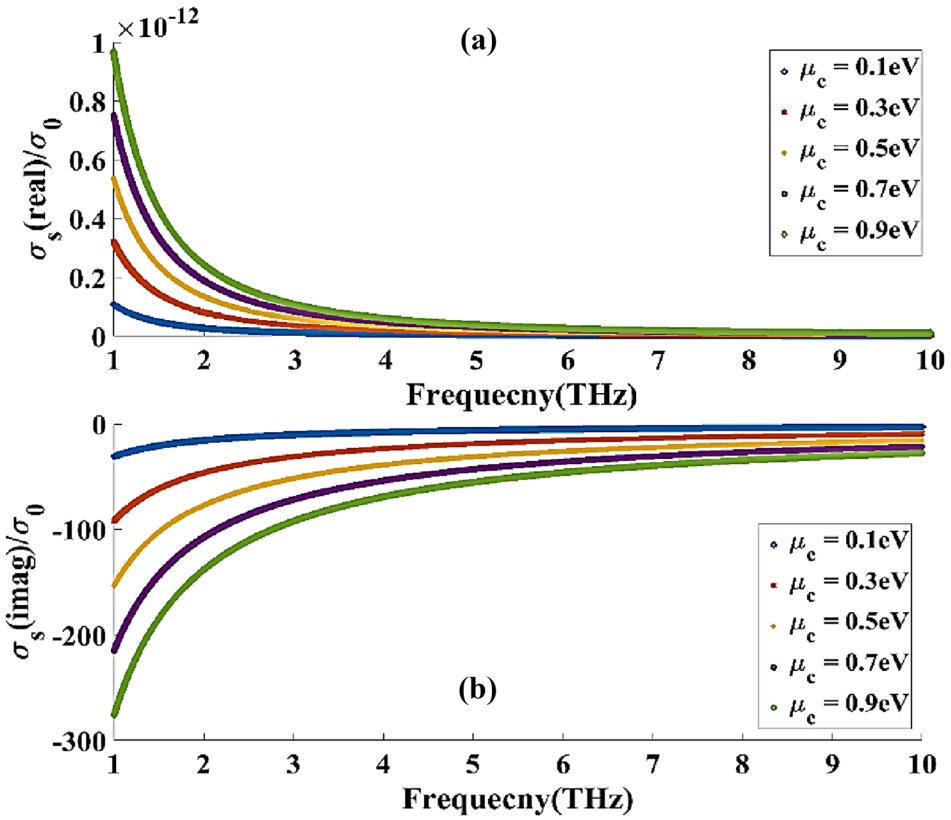

Fig. 2 Variation in graphene conductivity of **a** real and **b** imaginary parts for the different values of the graphene Fermi voltage/chemical potential

dimension L for identifying the resonance relation over 1–20 THz range. The comparative plot of the calculated equation and simulated results' points has been shown in Fig. 2e. We have considered the resonance points to estimate the proposed approximation equations while short-band absorption generated at a higher value of L and f has been neglected for calculation. We have identified the operating bandwidth and its resonating frequency with the initial trial and error method. In this simulation, we have set the chemical potential value of the graphene sheet as 0.9 eV. We have simulated the same structure with the different sizes of the structure L. We have found that the resonating frequency is fitted with the dimension as per Eqs. (5–7). The curve fitting equation has been calculated from the results that we identified from the simulated results. The curve fitting equation will just show the variation in resonating frequency with respect to the size of the proposed structure. It also needs to keep in mind that the resonance band is not continuous over the range of 1–20 THz because the value of the graphene sheet's chemical potential is set as 0.9 eV. We can still identify the resonance at any point between the specific frequency range and identify the resonance of side frequency by varying the graphene sheet's chemical potential. It is also identified the behavior of different physical parameter values that affected the resonance such as width of graphene and unit cell dimensions.

Amplitude variation in (a) T_{xx} and (b) R_{xx} for NGP structure. Amplitude variation in (c) T_{xx} and (d) R_{xx} for CGP structure. (e) The calculated curve fitting equation depends on the different resonating points for the NGP structure.

$$L = 0.7f^2 - 15.2f + 70.7, \tag{5}$$

$$L = -0.09f^3 + 2.8f^2 - 27.2f + 86.8, \tag{6}$$

$$L = 94.72\left(0.65^f\right). \tag{7}$$

It is also observed from the calculated resonance results that the resonance points are different for both NGP and CGP structures. The difference in T_{xx} amplitude for both of the structures has been presented in Fig. 4a. Figure 4b shows the variation in the phase difference for both structures. The phase variation is observed between − 180° and 180° in the NGP structure. While in the CGP structure, the phase variation has been observed between 100° and 180°.

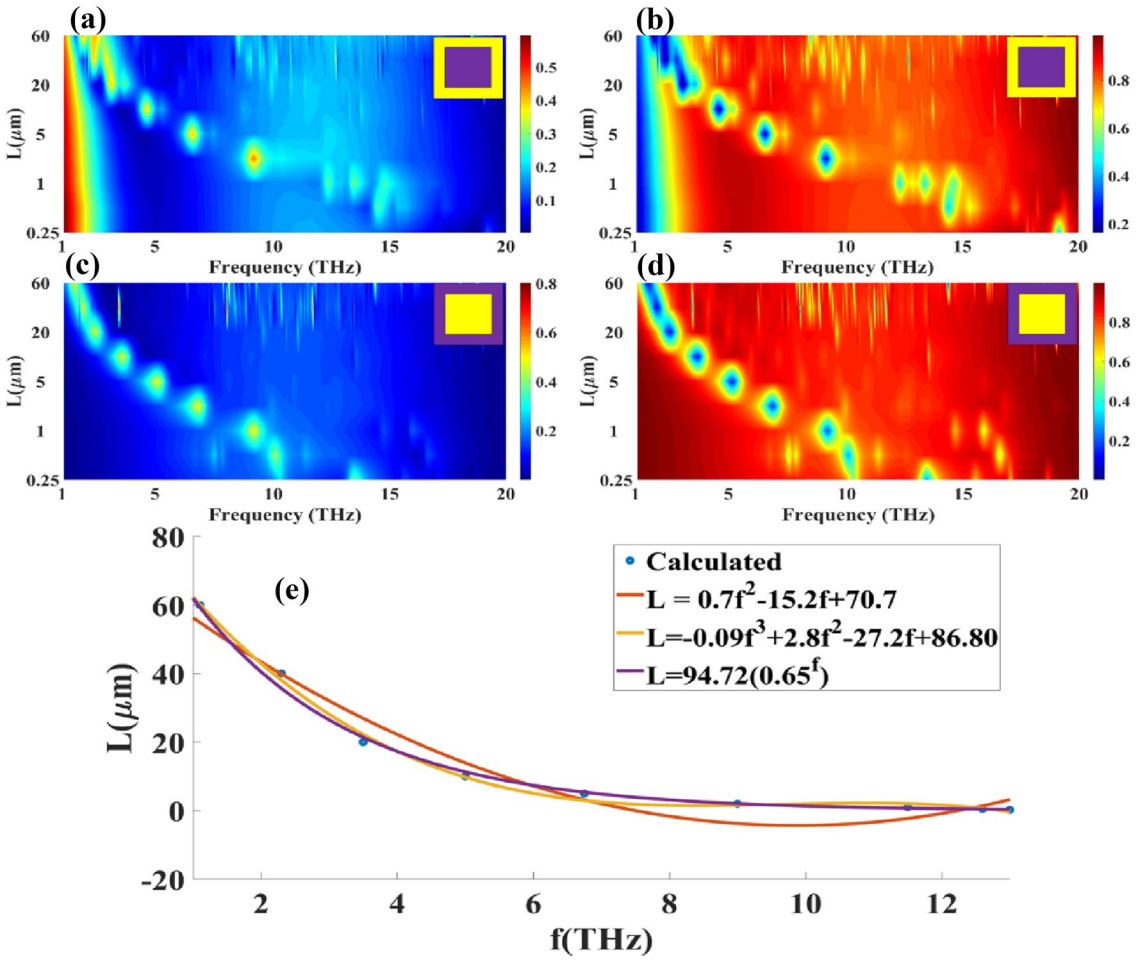

Fig. 3 Transmittance and reflectance coefficient amplitude for the multiple values of frequency and structure length

4 Polarization effect

The resonance band can be chosen by setting the different values of L and f, as shown in Fig. 3e. After setting the resonance values with L and f, a fixed resonating frequency can be identified from the same equation. We can further identify the variation in the resonance behavior by varying the graphene sheet's chemical potential. We have calculated the effect of the graphene chemical potential for the amplitude variation in T_{xx} and R_{xx} for NGP and CGP structure. The T_{xx} and R_{xx} response in Fig. 5 has been derived for the value of $L = 25$ µm. We can observe that the resonance band for the $L = 25$ µm is in between 1 and 5 THz for both the structures. Figure 5a and b represents the variation in T_{xx} and R_{xx} for NGP structure.

Similarly, Fig. 5c and d represents the variation in T_{xx} and R_{xx} for CGP structure. It is observed the notable amplitude and frequency shift for various chemical potential values. It is also observed that the amplitude of reflectance becomes more robust at the higher chemical potential of graphene as the charge concentration becomes more robust at higher chemical potential values. The main reason for generating a higher amplitude resonance is the strong dipole moment generated on the edge of the graphene surface. The variation in normalized electric field intensity for different chemical potentials is shown in Fig. 6. The variation in the phase Φ_{xx} for various chemical potential values for both of the structures has been demonstrated in Fig. 7. In the proposed polarizer structure, the $T_{xx} = T_{yy}$, $R_{xx} = R_{yy}$ and $\Phi_{xx} = \Phi_{yy}$ as the squared graphene patch geometry has been chosen.

5 Cross-polarization and PCR

The polarization conversion rate has been defined as $\mathrm{PCR} = \left|T_{xy}\right|^2 / \left[\left|T_{xx}\right|^2 + \left|T_{xy}\right|^2\right]$ [21] to reveal the performance of the proposed polarizer as a behavior of cross-polarization. The PCR for the X–Y cross-polarization for NGP and CGP structure is shown in Fig. 8. The calculated

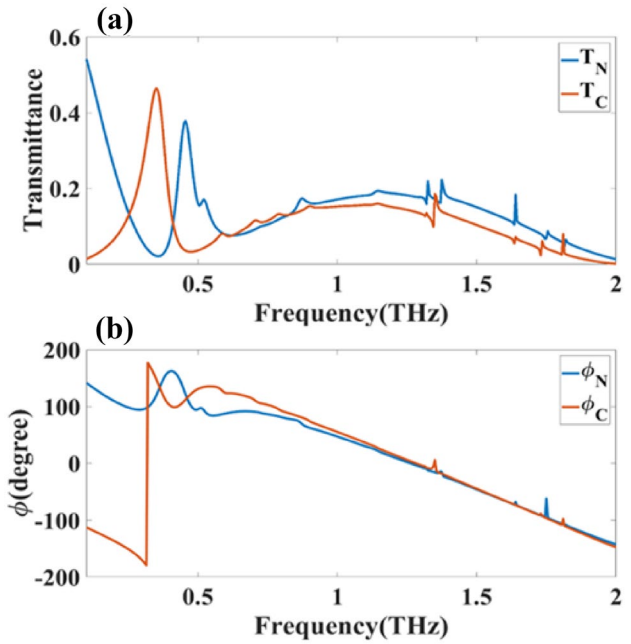

Fig. 4 Calculated differences in **a** transmittance and **b** phase variation response for NGP and CGP structures

transmittance coefficient T_{xx} and T_{xy} for co-polarization and cross-polarization has been demonstrated in Fig. 8a for NGP and Fig. 8c for CGP. The calculated PCR and $\Delta\Phi = \Phi_{xx} - \Phi_{xy}$ are presented in Fig. 8b and d for NGP and CGP structures. We have observed that PCR values are > 0.9 for the resonating frequency.

The phase difference is observed between − 300° and 200° in the NGP structure. While the phase difference of − 150°–50° in CGP structure. Furthermore, the proposed PCR values also can be tunable for the different chemical potential values. This effect will make the behavior of elliptical polarization conversion. The high contrast in the co-polarizer structure generated a dipole moment where the entire wave passed through the structure in the same direction as the incident wave. While the low contrast in cross-polarization response shows the minimum values, the loss in the transmitted wave is due to the large ohmic loss in graphene. We derive the PCR from the co- and cross-polarization. Once the PCR values reach > 90% value, the phase difference changes to − 300°–200° in the NGP structure and − 150°–50° in CGP structure. This variation in the angle makes overall behavior in circular/elliptical polarization.

We have also calculated the effect of the physical parameters $g_1 = g_2$ (squared graphene patch) for the frequency range from 1 to 10 THz. The effect of squared patch geometry for the size variation $g_1 = g_2 = 12$–24 μm has been presented in Fig. 8. Figure 8a and b presents the amplitude variation in T_{xx} and R_{xx} for the NGP structure, while Fig. 9c

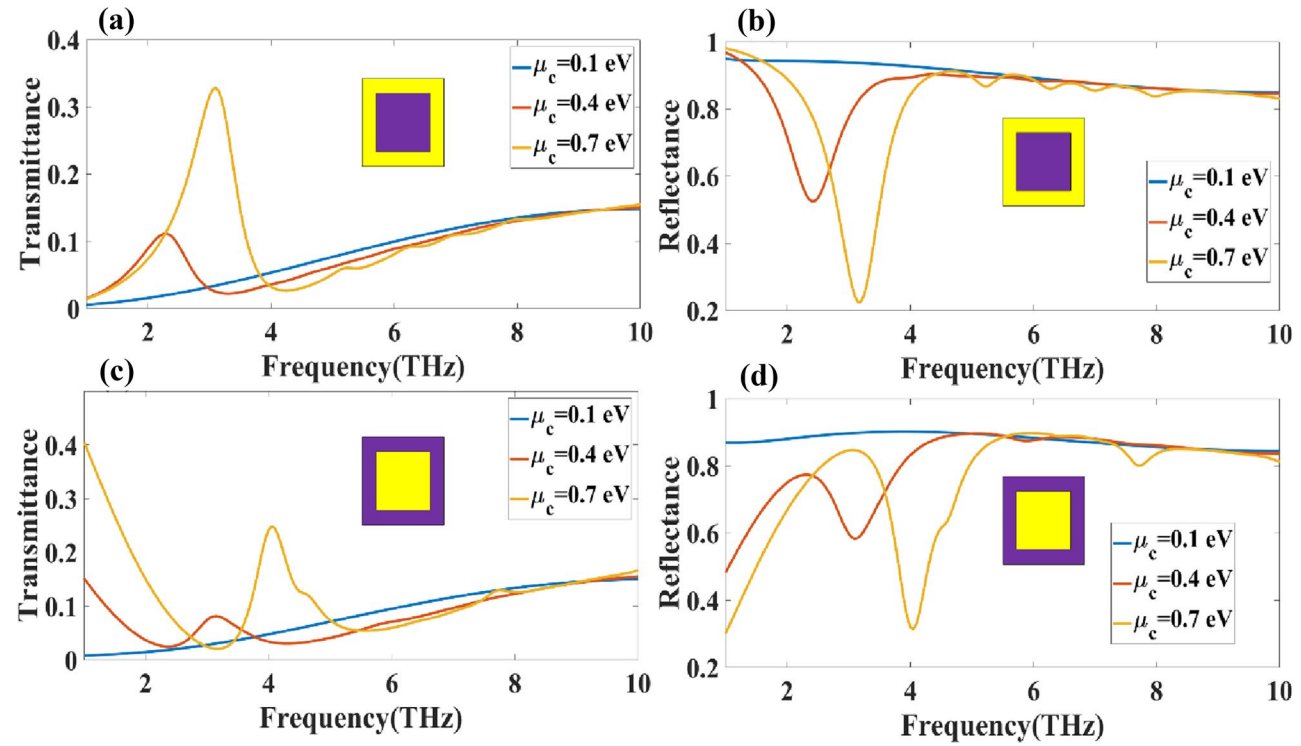

Fig. 5 Calculated variation in T_{xx} and R_{xx} for various graphene chemical potential values. **a** T_{xx} and **b** R_{xx} amplitude variation for NGP. **c** T_{xx} and **d** R_{xx} amplitude variation for CGP structure

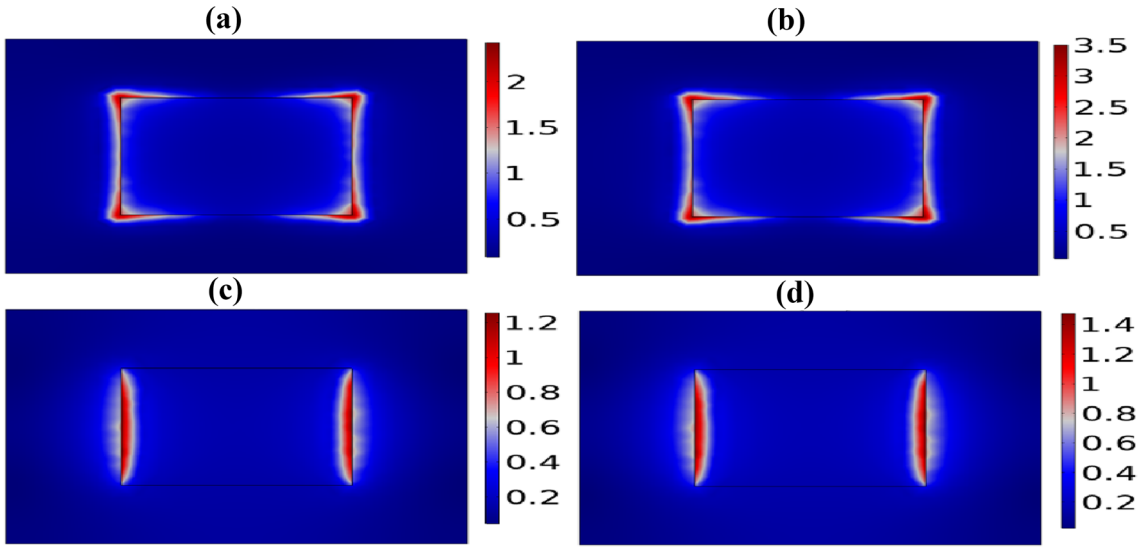

Fig. 6 Normalized electric field intensity for **a** $\mu_c = 0.4$ eV and frequency = 2.3 THz, **b** $\mu_c = 0.7$ eV and frequency = 3.1 THz for CGP structure and **c** $\mu_c = 0.4$ eV and frequency = 2.3 THz, **d** $\mu_c = 0.7$ eV and frequency = 3.1 THz for CGP structure

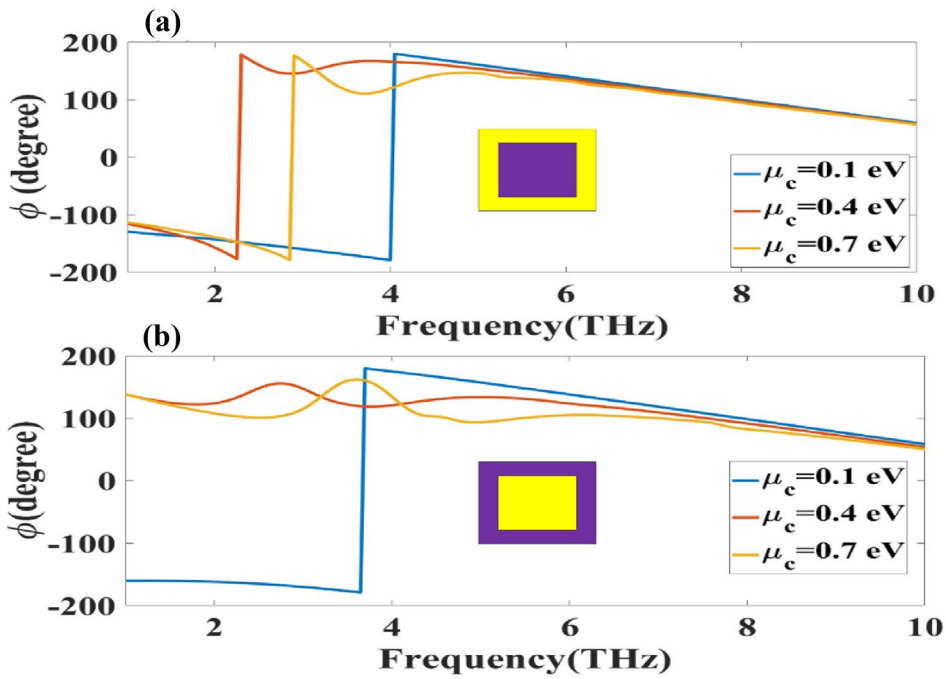

Fig. 7 Calculated variation in Φ_{xx} for different graphene chemical potential values. Φ_{xx} variation for **a** NGP and **b** CGP structures

and d shows the amplitude variation in T_{xx} and R_{xx} for CGP structure. It is observed that the resonance shift is changing over the 1–10 THz frequency spectrum for the CGP structure. Size variation in NGP offers the polariser's tunability over 1–5 THz with the different patch sizes, while size variation of g_1 in CGP structure provides a wide band of tunability ranging from 1 to 10 THz of the frequency range. We can also observe that the effect of the g_1 dimension is negligible near the resonance peak for the NGP structure, while the resonance in CGP structure depends on the dimension of g_1. We have also identified the reflectance and transmittance behavior of the rectangular patch with the dimension condition ($g_1 \neq g_2$). We have set $g_1 = 12$ µm, and $g = g_2$ is varying in the range of 2–10 µm. The effect in T_{xx} and R_{xx} has been reported in Fig. 10. It is observed variation of ~ 2–3 THz in resonance shift for the different values of g in both structures.

This research helps to identify the initial conditions for designing the basic single-layer graphene-based polarizer. The proposed polarizer is tunable for the far-infrared frequency

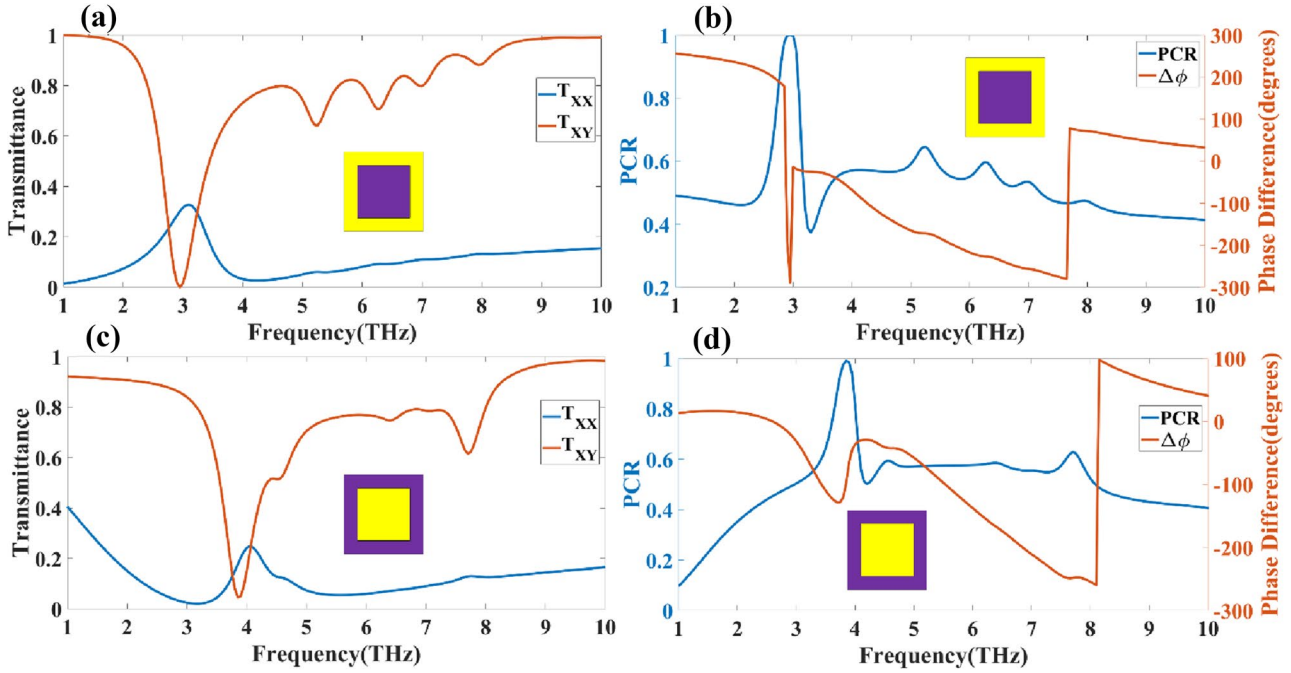

Fig. 8 Difference in resonance amplitude for co-polarizer condition (T_{xx}) and cross-polarizer condition (T_{xy}). **a** Calculated transmittance amplitude of T_{xx} and T_{xy} for NGP structure. **b** Variation in PCR and $\Delta\phi$ over a frequency range from 1 to 10 THz for NGP structure. **c** Calculated transmittance amplitude of T_{xx} and T_{xy} for CGP structure. **d** Variation in PCR and $\Delta\phi$ frequency range from 1 to 10 THz for CGP structure

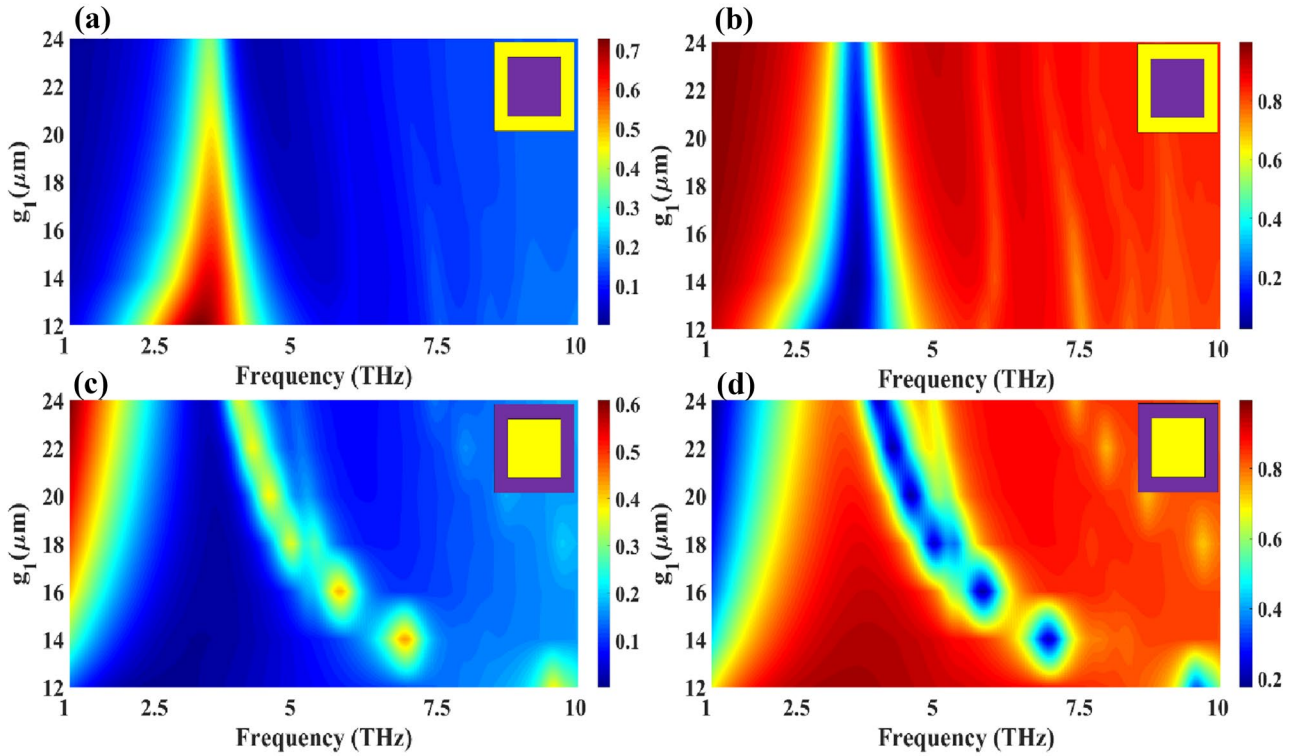

Fig. 9 Calculated variation in the T_{xx} and R_{xx} for graphene squared patch size ($g_1 = g_2$). Variation in **a** T_{xx} and **b** R_{xx} for NGP structure. Variation in **c** T_{xx} and **d** R_{xx} for CGP structure

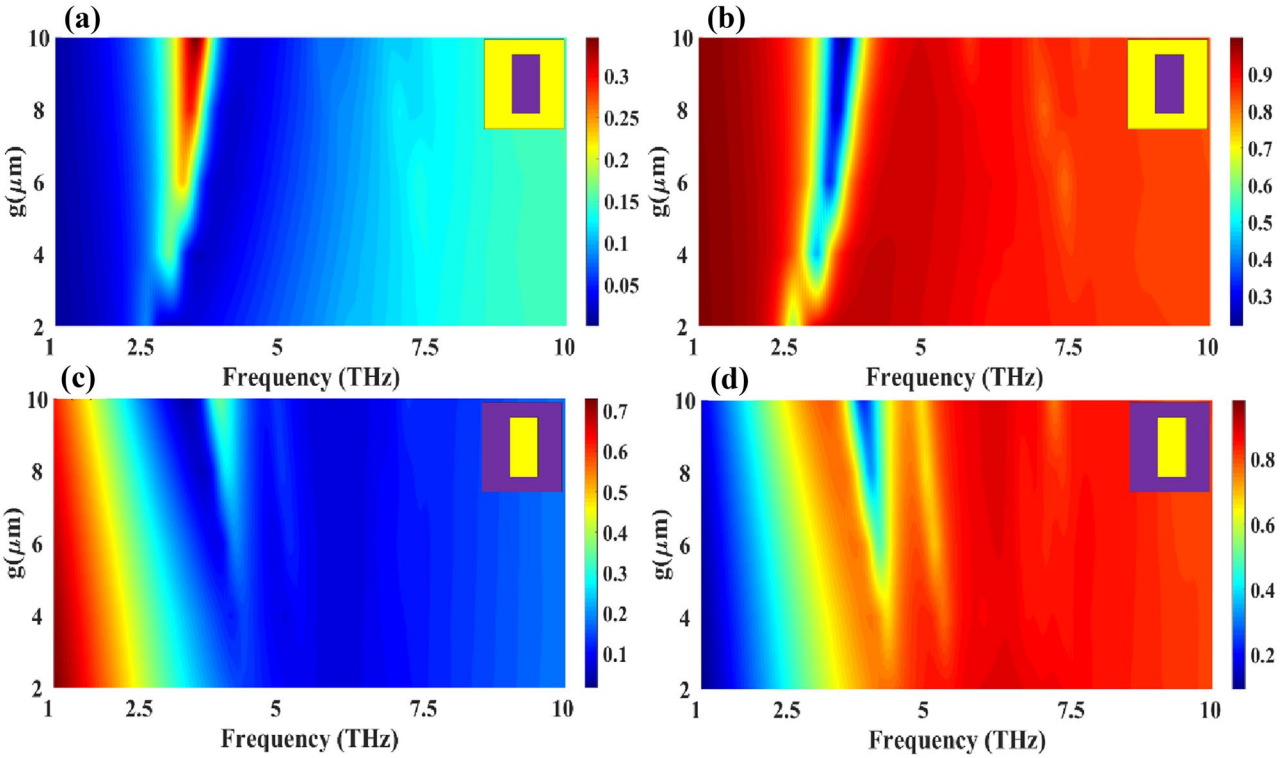

Fig. 10 Calculated variation in the T_{xx} and R_{xx} for graphene rectangular patch size ($g_1 \neq g_2$). The values of $g_1 = 12$ μm and $g = g_2$ vary in the range of 2–10 μm. Variation in **a** T_{xx} and **b** R_{xx} for NGP structure. Variation in **c** T_{xx} and **d** R_{xx} for CGP structure

Table 1 Comparative analysis of the proposed structure with the previously reported structures

Ref.	Type of graphene layer	Structure material	Operating band	Dimensions ($W \times L \times H$) in μm^3	Max. transmittance (%)
This structure	Single layer	Graphene dielectric	1–10	(25 × 25 × 5)	70
[22]	Single layer	Tantalum nitride	1.17–2.99	(70 × 70 × 25)	40
[23]	Single layer	Graphene silica	1–4	(4 × 4 × 0.25)	25
[24]	Single layer	Graphene dielectric gold	0.4–1	(120 × 120 × 59)	60
[25]	Multi-layer	Metal	0.76–1.48	(100 × 100 × 26)	30
[26]	Multi-layer	Metal	0.7–2.5	(105 × 105 × 25)	20
[27]	Single layer	Metal	1.6–5	(200 × 200 × 90)	45
[28]	Single layer	Graphene dielectric silica	0.6–2.6	(16 × 16 × 25)	22
[29]	Multi-layer	Graphene	1.65–4.35	(15 × 15 × 19)	75

spectrum. The polarization effect can be modified by changing the size of the single graphene sheet. It is easy to fabricate as it contains a single-layer graphene sheet on a silica substrate. The comparative analysis of the proposed structure with the previously reported structures is shown in Table 1. This structure is compared in terms of the numbers of graphene layers, the material used, operating band, dimensions, and maximum transmittance values. It is observed from the comparative analysis that the proposed structure is easy to form with a simple patch-shaped rectangular structure that operates on a wide band of the THz frequency spectrum.

6 Conclusion

In conclusion, we presented the graphene squared patch-based narrowband, and tunable metasurface polarizer for the frequency range lies in the far-infrared region. This

graphene-based structure has been identified for the two geometries on normal and complementary of the same structure. We have presented the possible dimension approximation equation for identifying the resonance frequency and its structure size. Furthermore, we have calculated and explained the different physical parameters proposed structure to determine the behavior of polarizer structure. The proposed polarizer device is tunable by various values of graphene chemical potential. The calculated PCR is > 0.9 for the resonating point, showing the linear to circular polarization conversion. The proposed numerical study gives the overall idea about the dimension approximation and tunable polarization effect over the 1–20 THz frequency range. The proposed polarizer can be easily fabricated using conventional methods because it does not require a complex structure to engrave the graphene sheet. Ultrathin design and tunable behavior of t proposed structure can be employed in many optoelectronics and photonics applications.

Acknowledgements This study was funded by the Deanship of Scientific Research, Taif University Researchers Supporting Project number (TURSP-2020/08), Taif University, Taif, Saudi Arabia.

Declarations

Conflict of interest The authors declare no conflict of interest.

References

1. K.P. Loh, Q. Bao, P.K. Ang, J. Yang, The chemistry of graphene. J. Mater. Chem. **20**(12), 2277–2289 (2010)
2. A.K. Geim, K.S. Novoselov, The rise of graphene, in *Nanoscience and technology: a collection of reviews from nature journals*. (World Scientific Publishing Co., Singapore, 2009), pp. 11–19
3. K.S. Novoselov, V.I. Fal'Ko, L. Colombo, P.R. Gellert, M.G. Schwab, K. Kim, A roadmap for graphene. Nature **490**(7419), 192–200 (2012)
4. X. Huang, X. Qi, F. Boey, H. Zhang, Graphene-based composites. Chem. Soc. Rev. **41**(2), 666–686 (2012)
5. C.N.R. Rao, K. Biswas, K.S. Subrahmanyam, A. Govindaraj, Graphene, the new nanocarbon. J. Mater. Chem. **19**(17), 2457–2469 (2009)
6. C. Chung, Y.K. Kim, D. Shin, S.R. Ryoo, B.H. Hong, D.H. Min, Biomedical applications of graphene and graphene oxide. Acc. Chem. Res. **46**(10), 2211–2224 (2013)
7. A.V. Kildishev, A. Boltasseva, V.M. Shalaev, Planar photonics with metasurfaces. Science **339**, 1232009 (2013)
8. H.-H. Hsiao, C.H. Chu, D.P. Tsai, Fundamentals and applications of metasurfaces. Small Methods **1**(4), 1600064 (2017)
9. S.B. Glybovski, S.A. Tretyakov, P.A. Belov, Y.S. Kivshar, C.R. Simovski, Metasurfaces: from microwaves to visible. Phys. Rep. **634**, 1–72 (2016)
10. A. Li, S. Singh, D. Sievenpiper, Metasurfaces and their applications. Nanophotonics **7**(6), 989–1011 (2018)
11. A.E. Minovich, A.E. Miroshnichenko, A.Y. Bykov, T.V. Murzina, D.N. Neshev, Y.S. Kivshar, Functional and nonlinear optical metasurfaces. Laser Photonics Rev. **9**(2), 195–213 (2015)
12. V. Dave, V. Sorathiya, T. Guo, S.K. Patel, Graphene based tunable broadband far-infrared absorber. Superlattices Microstruct. **124**, 113–120 (2018)
13. V. Sorathiya, V. Dave, Numerical study of a high negative refractive index based tunable metamaterial structure by graphene split ring resonator for far infrared frequency. Opt. Commun. **456**, 124581 (2020)
14. S.K. Patel, V. Sorathiya, S. Lavadiya, T.K. Nguyen, V. Dhasarathan, Polarization insensitive graphene-based tunable frequency selective surface for far-infrared frequency spectrum. Phys. E Lowdimensional Syst. Nanostruct. **120**, 114049 (2020)
15. W. Guo, et al., Design of infrared polarizer based on sub-wavelength metal wire grid, in *Eighth international symposium on precision engineering measurement and instrumentation,* 2013, vol. 8759, p. 87593I
16. S.K. Patel, V. Sorathiya, S. Lavadiya, L. Thomas, T.K. Nguyen, V. Dhasarathan, Multi-layered graphene silica-based tunable absorber for infrared wavelength based on circuit theory approach. Plasmonics **15**(6), 1767–1779 (2020)
17. H.N. Rutt, A low-cost, ultra-wide-range infrared polarizer. Meas. Sci. Technol. **6**(8), 1124–1132 (1995)
18. G.W. Hanson, Dyadic Green's functions and guided surface waves for a surface conductivity model of graphene. J. Appl. Phys. **103**(6), 064302 (2008)
19. H. Cheng, S. Chen, P. Yu, J. Li, L. Deng, J. Tian, Mid-infrared tunable optical polarization converter composed of asymmetric graphene nanocrosses. Opt. Lett. **38**(9), 1567 (2013)
20. J. Ding et al., Mid-infrared tunable dual-frequency cross polarization converters using graphene-based l-shaped nanoslot array. Plasmonics **10**(2), 351–356 (2015)
21. J. Hao et al., Optical metamaterial for polarization control. Phys. Rev. A **80**(2), 023807 (2009)
22. G. Deng, J. Yang, Z. Yin, Broadband terahertz metamaterial absorber based on tantalum nitride. Appl. Opt. **56**(9), 2449 (2017)
23. E. Gao et al., Dynamically tunable dual plasmon-induced transparency and absorption based on a single-layer patterned graphene metamaterial. Opt. Express **27**(10), 13884 (2019)
24. X. Yu, X. Gao, W. Qiao, L. Wen, W. Yang, Broadband tunable polarization converter realized by graphene-based metamaterial. IEEE Photonics Technol. Lett. **28**(21), 2399–2402 (2016)
25. S. Liu, H. Chen, T.J. Cui, A broadband terahertz absorber using multi-layer stacked bars. Appl. Phys. Lett. **106**(15), 1–6 (2015)
26. C. Shi et al., Compact broadband terahertz perfect absorber based on multi-interference and diffraction effects. IEEE Trans. Terahertz Sci. Technol. **6**(1), 40–44 (2016)
27. X. Liu, Q. Zhang, X. Cui, Ultra-broadband polarization-independent wide-angle THz absorber based on plasmonic resonances in semiconductor square nut-shaped metamaterials. Plasmonics **12**(4), 1137–1144 (2017)
28. J. Zhu, S. Li, L. Deng, C. Zhang, Y. Yang, H. Zhu, Broadband tunable terahertz polarization converter based on a sinusoidally-slotted graphene metamaterial. Opt. Mater. Express **8**(5), 1164 (2018)
29. A. Fardoost, F.G. Vanani, A. Amirhosseini, R. Safian, Design of a multilayer graphene-based ultrawideband terahertz absorber. IEEE Trans. Nanotechnol. **16**(1), 68–74 (2017)